International Journal of Greenhouse Gas Control 136 (2024) 104192

Contents lists available at ScienceDirect

International Journal of Greenhouse Gas Control

journal homepage: www.elsevier.com/locate/ijggc

New and accurate thermodynamic property data of CO_2-EGS relevant working fluids with data fitted to existing thermodynamic models

Jacob Stang [a], Anders Austegard [a], Yannick Jooss [a], Maciej Szymanek [b,*], Anna Sowiżdżał [b]

[a] SINTEF Energy Research, P.O. Box 4761 Torgarden, Trondheim NO-7465, Norway
[b] Faculty of Geology, Geophysics and Environmental Protection, AGH University of Krakow, Al. Adama Mickiewicza 30, Kraków 30-059, Poland

ARTICLE INFO

Keywords:
Vapor-liquid equilibrium
Equation of state
Water
Carbon dioxide
Enhanced geothermal systems

ABSTRACT

The article presents a new setup for the accurate measurements of the phase behaviour of CO_2 mixtures relevant to CCS as well as a CO_2-H_2O working fluid for EGS, designed to cover the temperature range from -60 to 200 °C and up to 100 MPa in pressure. Included in the article are a description of the experimental setup, methodology, and results of the experimental campaign conducted in the SINTEF Energy Research labs for the EnerGizerS project. Phase equilibrium of the CO_2-water system has been investigated at the temperature of 50 °C and pressures between 1 and 17.5 MPa, using the analytical isothermal technique. These measurements are compared and verified against the existing data, followed by a presentation of the fit of GERG-2008/EOS-CG for CO_2 and H_2O. The maximum mole fraction of water in the CO_2—H_2O mixture at measured conditions should not exceed 0.35 % and even less than 0.3481 % at 7.8 MPa to maintain the vapour phase of the mixture. The accuracy with respect to GERG-2008/EOS-CG varies from 1.044 % to 10.683 % near the critical values of sCO_2. The estimated uncertainty of the setup is 31 mK for temperature measurements, from 0.4 to 2.5 kPa for pressure measurements and from 0.2 to 2.1 % of total combined relative uncertainty as regards the mole fraction. Despite the fact that the EGS reservoir could reach conditions above 150 °C and 50 MPa, lower values were adopted to validate the setup at 50 °C. Knowledge gaps at higher pressure and temperature values are still in dire need of filling.

Introduction

Carbon dioxide (CO_2) is one of the main greenhouse gases affecting climate change, but it also has wide commercial and industrial applications. The most obvious industrial application is beverage carbonation. Further uses of carbon dioxide in the food industry include cooling and freezing food or protective atmosphere packaging. In the last decade, supercritical carbon dioxide assisted processes have arisen as innovative alternatives to particle design in the pharmaceutical industry (Honarvar et al., 2023). CO_2 is also used in other industries, such as agriculture, chemical, petrochemical, metal processing or construction. In terms of large-scale application, methanol, polymers, urea synthesis and mineral carbonation technologies are leading the race (Kim et al., 2022).

CO_2 is part of the carbon cycle in nature, as a product of combustion and respiration. It is also harmful to humans in excessive quantities. Carbon dioxide capture and storage, which can reduce the amount of carbon dioxide gas in the atmosphere, is used to prevent large amounts of carbon dioxide from being emitted into the atmosphere from point sources of pollution. The captured gas can be deposited in underground reservoirs and stored in a stable mineral form or reused in industrial applications (Leventaki et al., 2023). Carbon Capture and Storage (CCS) is an efficient method to mitigate carbon dioxide (CO_2) emissions into the atmosphere (Noorani et al., 2021). Geological sequestration of CO_2 is a process in which CO_2 is separated from industrial or other energy sources, and then transported and injected into deep geological strata, where it is isolated from the atmosphere. Typically, these can include deep saline aquifers, depleted oil and gas fields as well as coal deposits (Hou et al., 2022).

However, CO_2 has excellent transport properties and could be used to transport energy from deep within the Earth. In deep reservoir zones, geothermal energy is accumulated in dry rocks that do not contain water, which is a natural energy carrier. The energy cannot be extracted using typical hydrogeothermal systems, the most commonly applied throughout the world, with well-recognised extraction technology. However, it is technically possible to extract the energy accumulated in hot dry rocks using the Enhanced Geothermal System (EGS). This is done by artificially increasing the hydraulic capacity of the geothermal

* Corresponding author.
E-mail address: maszyman@agh.edu.pl (M. Szymanek).

https://doi.org/10.1016/j.ijggc.2024.104192
Received 9 November 2023; Received in revised form 24 May 2024; Accepted 26 June 2024
Available online 10 July 2024

reservoir, introducing a working fluid, as an energy carrier, into the reservoir and then transporting it to a power plant or a CHP plant (Tester et al., 2006). The standard working fluid in the EGS technology is water (Aminu et al., 2017), but research is underway regarding the use of carbon dioxide as a working fluid (CO_2-EGS). There are numerous indications of the potential benefits of using CO_2 in EGS applications (Zhang et al., 2016; Olasolo et al., 2018; Pruess, 2008; Cui et al., 2018), due to its good thermodynamic properties and the need to reduce carbon dioxide emissions into the atmosphere. CO_2 is less effective as a solvent for most rock minerals and its larger compression and expansion properties reflect the strong natural buoyance force that yields larger self-propelled flow velocities and a lower power consumption by the fluid circulation system. CO_2 has a lower viscosity, resulting in higher mobility and higher flow capacity, higher mass rate and partially compensates for its lower mass heat capacity (when compared with water) through higher flow rates (Tagliaferri et al., 2022).

CO_2-EGS uses carbon dioxide as the working medium, which is injected into the reservoir. As the reservoir is never fully dry, but contains a certain quantity of water, a mixing of water and CO_2 takes place. The working fluid circulating in the system will almost always be a water-CO_2 mixture. The percentage content of each fluid depends on a number of factors, including the petrophysical parameters of the rock, temperature and pressure. The objective of the research presented in this article is to understand the behaviour of the working fluid in a CO_2-EGS system. Therefore, the motivation for choosing a mixture of CO_2 and water is the realisation that, in some cases, there may be a small quantity of water in the reservoir, and some water may also enter the CO_2 fluid during the injection. It is worth noting that the fluid properties of CO_2-rich fluids depend strongly on pressure and temperature. While this is true for all properties, it could have particularly significant consequences for the phase equilibrium, where a second phase could lead to the breakdown of rotating machines or, in the case of water, also serious corrosion. One consequence could for instance be that CO_2 absorbs water in the reservoir, which could then condense to a second phase as heat is extracted from the fluid on the surface side of the EGS process. Therefore, knowing exactly the shape of these phase curves is necessary and interesting in the context of the operation of CO_2-EGS systems, and an understanding of these phenomena should be reflected in the design processes of EGS plants, including the surface part.

EGS systems using carbon dioxide instead of water are gaining interest worldwide due to the possibility of geological storage of carbon dioxide in the process of obtaining geothermal energy. CO_2-EGS technology makes it possible to harvest renewable energy as part of the international efforts aimed at mitigating anthropogenic climate change. The proposed solution contributes to climate protection by providing clean geothermal energy while eliminating carbon dioxide emissions from fossil fuel combustion. Supercritical CO_2 (sCO_2) may be utilised as the circulating heat exchange fluid in combination with the organic Rankine cycle (ORC). The circulating CO_2 could also be used directly as the working fluid in the CO_2 power cycle (e.g. the Brayton cycle) (Gładysz et al., 2020). The subject of the use of CO_2 as a medium in EGS is currently being investigated by an international consortium within the EnerGizerS project (Sowiżdżał et al., 2021; Pająk et al., 2021). The main goal of the project is the development of EGS with CO_2 instead of water as the working fluid. The possibility of building EGS systems using CO_2 as the working fluid in Poland and Norway is analysed.

Currently, there are significant knowledge gaps regarding the thermodynamic properties of CO_2 mixed with relevant impurities for CO_2-EGS, and even larger ones regarding the transport properties and phase behaviour of certain components (Løvseth, 2021). Research studies are available concerning the solubility of water in carbon dioxide (Tabasinejad et al., 2011; Hou et al., 2013; Wang et al., 2018; Caumon et al., 2016) at high temperatures and pressures, however some of the data are in need of confirmation. Furthermore, most studies provide phase equilibrium data derived from measurements of CO_2 solubility in water at low pressures. The existing data as well as the identified gaps in thermodynamic models describing the PVTxy-behaviour of CO_2—H_2O mixtures were summarised in work of Aasen et al. (2017). This article contains a detailed study of CO_2 + water thermodynamic data. A considerable amount of vapor-liquid equilibrium data has been found for this system, however almost all of the data came from CO_2 solubility measurements in water at low pressures. The poor fit of the data when extrapolating different models poses another problem. In contrast, the measurements of Tabasinejad et al. (2011) extend to a pressure of 124 MPa with four isotherms between 423 and 478 K. However, the data require confirmation, due to the difficulty in conducting the measurements. The measurements of Hou et al. (2013) extend up to a pressure of 17.5 MPa over 7 isotherms between 298 and 448 K. Two more studies concerning high pressure water solubility in CO_2 have been published. Wang et al. (2018), for pressures between 10 and 50 MPa and temperatures between 313 and 473 K, and Caumon et al. (2016) – up to 2 MPa and 373 K. All studies demonstrate the challenges of obtaining accurate results at high pressures, highlighting the need for further research to provide highly accurate phase equilibrium data.

This study presents a new apparatus and vapour-liquid equilibrium (VLE) measurements for the CO_2 + H_2O system. The setup is located in the SINTEF Energy Research laboratory in Norway. It is also a part of The European CCUS Research Infrastructure – ECCSEL ERIC. The results of this study come from the first experiments conducted in the facility. Five institutions from Poland and Norway: AGH University of Krakow, SINTEF Energy Research, Mineral and Energy Economy Research Institute of the Polish Academy of Sciences, Norwegian University of Science and Technology and Exergon have formed a consortium to analyse the efficiency of Enhanced Geothermal Systems using supercritical carbon dioxide as a working fluid (CO_2-EGS).

Experimental apparatus

Apparatus

A High-Pressure and Complex Phase Equilibrium (HPC-PE) facility has been developed at SINTEF Energy Research, specifically designed for highly accurate measurements of vapor-liquid equilibrium (VLE). The new setup is similar to the CO_2Mix facility, described by Stang et al. (2013), but with a wider range of temperature and pressure values, from -60 °C to 200 °C and from 4 to 1000 bar. A variety of fluids including toxic, flammable, sulphur-containing, and corrosive mixtures can be analysed. Research areas where HPC-PE could be used include phase and chemical equilibrium measurements, thermodynamics, chemistry/geochemistry, physical processes, fluid transport properties, modelling and others. Both CCUS and EGS applications are suitable for the conditions mentioned above (ECCSEL ERIC 2023).

The phase equilibrium is measured using the analytical isothermal technique described by Dohrn et al. (2010). Phase equilibrium is established in the cell at a given pressure and temperature, then the gas and liquid composition is analysed in a gas chromatograph (GC). The crucial element of the setup is the VLE cell, where components are injected, and the phase equilibrium is established.

A general diagram of the setup is presented in Fig. 1.

VLE cell

The main part of the setup is a VLE cell made of Inconel 625, as shown in Fig. 2.

It consists of a horizontal cylinder with a sapphire glass window for visual inspection, bellows for volume compensation during sampling and temperature sensors. The cell is provided with three independent injection lines. The first injection point was used for CO_2 (primary component – it can be also a different component, for this study CO_2 was used), the second one was used for water/brine, the third injection point was used for secondary gas components. There are two independent lines for draining and evacuating the cell. Three independent sampling

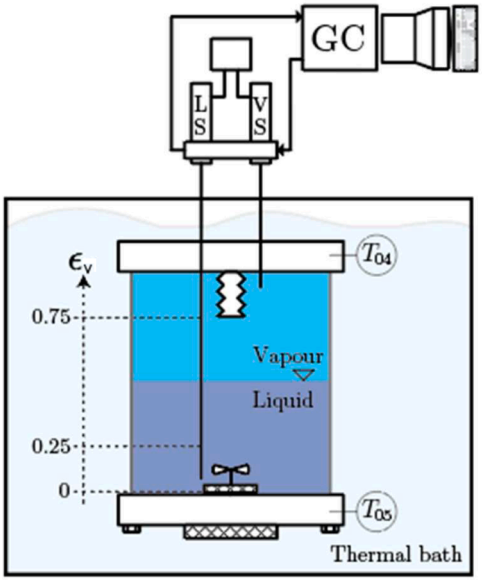

Fig. 1. General diagram of the setup (GC – Gas chromatograph, LS – liquid sample, VS – vapour sample, T04 – platinum resistance thermometer PT-100, T05 – platinum resistance thermometer SPRT, ϵ_V – fractional location of bellows and stirrer in the volume of the VLE cell).

lines are located at different heights inside the cell – one for the liquid samples located at the bottom of the cell, one for the vapour samples in the top of the cell, and the third one for sampling of a secondary liquid phase in the central point of the cell. Bellows, with a working volume of 10 ml, are mounted inside the cell and provide pressure control during stirring and sampling. The bellows are filled with an appropriate liquid in the quantity controlled by an external syringe pump.

A magnetic stirrer inside the cell provides for a good distribution of the mixture, facilitates evacuation, and most importantly, provides an easier and faster way of establishing the equilibrium. The RPM of the stirrer is selected by the operator, based on their experience. The maximum RPM value should not exceed over 800 for safety reasons. The stirrer has a propel in both the upper and lower parts to ensure proper mixing in both phases. The temperature sensor in the top part of the cell is a Fluke model 5686 glass capsule Standard Platinum Resistance Thermometer (SPRT), and the temperature sensor in the bottom of the cell is a Fluke model 5615–9-B PT-100. Both are mounted inside the cell wall at two different heights. The temperature sensors are connected to a WIKA ASL model CTS9000 multiplexer and interrogated using a WIKA ASL model CTR6500 thermometry bridge. A hole for the Raman probe allows using spectroscopic methods for *in-situ* concentration measurements, however, such methods were not used in this study.

The pressure is measured by an array of 6 pressure transmitters (Keller PAA33X) to achieve a low uncertainty of the pressure measurement across the entire pressure range. The pressure transmitters are insulated from the corrosive fluids in the cell by a differential pressure transmitter (Rosemount 3551). A syringe pump connected to the pressure transmitter array keeps the pressure difference at zero during the measurements. A constant temperature is provided by submerging the cell into a highly precise thermostatic bath (Fluke Hart Scientific model 7080). The bath is filled with silicone oil (Dow Corning, Xiameter PMX-200, 50). The bath has a specified uniformity and stability better than 10 mK. All materials and parts are carefully selected to meet the requirements of durability and are resistant to toxic, explosive, sulphur-containing and corrosive mixtures at wide range of pressure and temperature.

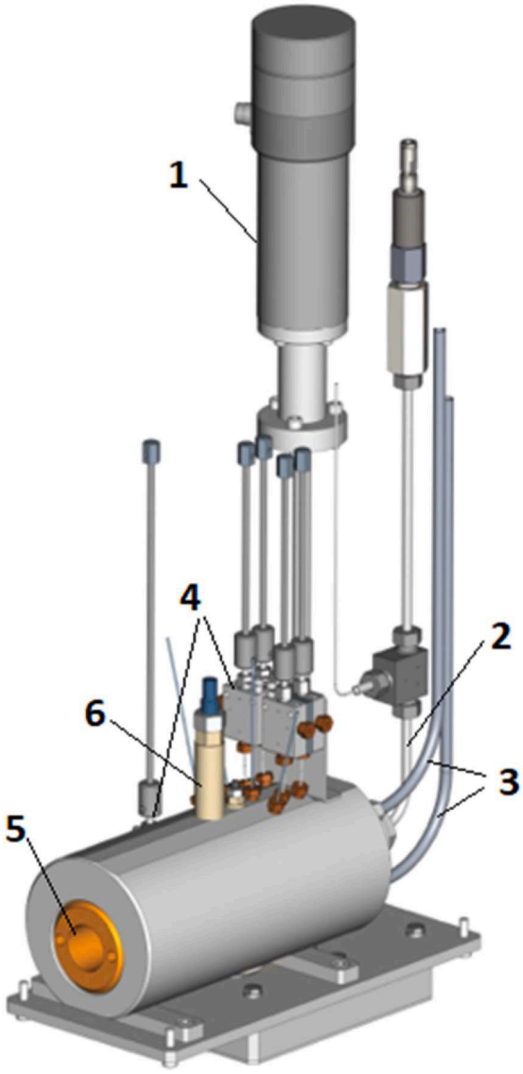

Fig. 2. VLE Cell. (1: Stirrer motor, 2: Tube with oil for the bellows, wires for bellows position sensing, 3: Tubes feeding wires to the SPRT (Standard Platinum Resistance Thermometer), 4: Valves close to the cell for gasses supply and cell evacuation, 5: Front glass of the cell, 6: Plug for future Raman probe).

Components injection

An important feature of the cell is the possibility of independent injection of different components. To inject the components, three PMHP 35–1000 and 50–1000 precise syringe pumps by Top Industrie are used. The injection process is controlled by the operator and software specially designed for HPC-PE. Water is purified by a Merck Milipore Direct-Q® 3 Water Purification System and a 3M™ Liqui-Cel™ SP-0.5 × 1 Series Membrane Contactor to remove oxygen. The final oxygen quantity should be less than 1 ppm before evacuation with a vacuum pump. The water is directed into an evacuated cylinder and further transferred to the syringe pump. The syringe pump is connected to a vacuum pump after filling with water to remove any traces of air that may have polluted the water during the process. After a flushing and evacuation of the cell, water is injected into the cell and a suitable water level is observed in the sapphire glass window. Typically, approximately 1/3 of the cell is filled with water. Next, CO_2 is injected while the stirrer is being operated until the desired cell pressure is achieved. The syringe pump can increase the cell pressure up to 1000 bar. The filling procedure for CO_2 is automated by the controlling software. The chemical properties of the components are presented in Table 1.

Table 1
Chemical properties of the components.

Chemical Name	CASRN	Source	Initial mole fraction purity	Purification method	Final mole fraction purity	Analysis
Carbon dioxide	124–38–9	Yara Praxair	0.999993	None	0.999993	None
Water	7732–18–5	N/A		Filter and evaporation	0.9999	None
Helium	7440–59–7	Linde	0.999999	None	0.999999	None

Temperature measurements and control

The measurements are taken along isotherms with the thermostatic bath set at a constant temperature, while the pressure is increased in steps. The heating and cooling of the bath is controlled by a temperature sensor in the bath fluid, while the cell temperature is measured in the cell wall at two locations.

All the parts and lines from the VLE cell to the GC, are heated and thermal-tracked, including tubing, valves, and sampling cylinders to avoid any condensation of the vapour extracted from the cell. The temperature is controlled in four different sections: between the liquid level and the outlet above the bath, from the VLE cell to the sampling cylinder, at the sample cylinder, and along the line from the sampling cylinder to the GC. Temperature readings are provided by thermocouples mounted on crucial elements. The temperature is set at a higher level compared to temperature of the oil bath/VLE cell, to avoid potential condensation which would affect the measurement.

Pressure measurements and control

Pressure measurements are performed using an array of 6 transmitters (supplied by Keller Druckmesstechnik, type PAA-33X/80794, with a range of 10, 30, 100, 200, 500 and 1000 bar, respectively) with the precision of 0.01 %. Transmitters are located in the reference circuit with nitrogen, while the connection with the VLE cell is provided by a membrane and a differential pressure controller. The pressure control circuit is separated from the rest of the apparatus to avoid damage by corrosive fluids and high temperatures. Total pressure is calculated as a sum of pressure readings of the differential pressure controller and the relevant pressure transmitter. The pressure in the nitrogen circuit is controlled by a separate syringe pump, to maintain the differential pressure at zero.

The purpose of the bellows mounted in the VLE cell is to compensate for the pressure drop and avoid affecting the accuracy during sampling. The bellows are controlled by a separate syringe pump filled with silicone oil. The syringe pump controls the cell pressure and compensates for the extracted volume during sampling.

Composition measurements

The chemical composition of both the vapour and the liquid (liquid samples were not taken in this study) phases are analysed using the gas chromatograph supplied by Agilent Technologies, model 7890B, equipped with a Supel-Q PLOT (30 m x 0.32 mm, average thickness 15 μm) with the CO_2 and water separated. Downstream of the column, a thermal conductivity detector (TCD) measures the temperature of the separated components.

Helium is used as a carrier gas. The GC oven with the column is heated to 100 °C and kept at a constant temperature during the entire duration of the analysis – 10 min. Each component has its own retention time, and as a result, the values are measured at different points in the process. The first peak on the chromatogram is nitrogen/oxygen, usually with a low height and surface area, the second one is carbon dioxide, which appears directly after the first peak, after that, the water peak is detected. Usually, the peaks conform to the Gaussian shape, however, the tail slope of the water peak is longer. In order not to extrapolate the total composition, the peak is cut at 4.2 min. Then, the GC outputs are analysed using the Python programming language, where the surface areas of the peaks are recalculated, and the area fraction for each component is calculated using the following formula:

$$X_{A\ c_1} = \frac{c_1}{(c_1 + c_2)} \cdot 100\%$$

Where:
X_A – area fraction
C_1, c_2 – component 1, component 2

The final composition after analysis can be calculated using the formula:

$$X_n = \frac{X_A}{X_A + R(100\% - X_A)}$$

Where:
X_n – mole fraction
R- response factor

The response factor determines the correlation between the area fraction and the mole fraction; this value should be stable in the entire range of area/mole fraction values. The response factor is calculated as a result of the GC calibration, as described in the Appendix.

Experimental procedures

Before commencing the experiment, the entire system must be appropriately prepared. That process involves an initial configuration of all the valves to their start positions, connection of the right gas cylinders, filling the water container and checking the sensors in the controlling software. Then, initial flushing and evacuation of the setup can start. Flushing and evacuation are completed before:

- Filling of a new reference mixture for GC calibration
- Phase equilibrium measurements of a new chemical system
- Before a planned stop and after a pause in the use of the apparatus

The gas lines from the primary gas cylinders via syringe pumps to the VLE cell (CO_2) and the reference pressure circuit (N_2) are also flushed and evacuated. After an initial flushing and evacuation, the pressure is increased to 5 bar, then released, and the lines are evacuated. This procedure is repeated twice.

The evacuation/flushing of the VLE cell and the lines from the syringe pumps follow the procedure: bellows are moved to the central position (half of the volume), the stirrer is set to 400 RPM and the system's pressure is reduced by ventilation (above 3 bar) and then vacuum is created. These conditions provide for a thorough evacuation of the cell. If the vacuum pressure is stable, CO_2 or N_2 is introduced to the cell to around 1 bar and the vacuum is created again. These steps are repeated one more time. After that, the cell is filled to approx. 4 bar and the stirrer can be turned off. The evacuation of the sampling cylinder and the lines from the VLE cell is a simple process and consists of filling them to 1 bar, followed by creating a vacuum 2 times at stable pressures. Flushing/evacuating of the syringe pump and the reference pressure circuit is similar to flushing/evacuating of the gas lines from the primary gas cylinders – the only exception is the opening/closing of the safety valves for each pressure transmitter, in the order from the lowest to highest range.

When the entire system is evacuated, the bellows are tested and the limit switches on both ends are checked to verify the working volume. Tests are performed at a low pressure, approx. 4 bar, to protect them in

case of failure. Pressure difference above 2 bar is destructive.

The bath must be filled with the correct fluid. The VLE cell can be submersed to the bath only if the fluid temperature is close to room temperature. The experiment can start when the temperature of the VLE cell reaches the desired temperature of the fluid. Lines and parts that require heating must also be at a stable temperature, just as the VLE cell. The injection of water to the VLE cell as the preparation phase of the experiment is controlled by the operator. Approximately 30 ml of water is injected to the cell at a flow rate of approx. 0.5 ml/min. An external camera enables monitoring the water level – it should be in the centre of the stirrer. Turning the stirrer on and off confirms the water level. The injection of CO_2 is controlled by software and operator. The software controls the operation of automated valves and the CO_2 syringe pump to obtain the desired cell pressure. The stirrer is operated during the injection of CO_2 to speed up the equilibration process. During the injection and equilibration, the temperature in the cell deviates from the bath temperature. Equilibrium is reached when the temperature is stable, the bellows are in a low-volume position, and the differential pressure between the cell and the pressure measurement circuit is zero. The stirrer is set to 800 RPM, and the bellows control the pressure. A stable equilibrium is established when the speed of the pump controlling the bellows is below the threshold value. After that, a gas sample is sent to the sample cylinder for analysis.

During stirring at 800 RPM, the shape of the gas/liquid interphase is a vortex. That ensures the mixing action reaches the VLE. Mixing at 400 RPM does not provide such effect. The behaviour of the mixture is visible on the camera. Pictures are presented in Fig. 3.

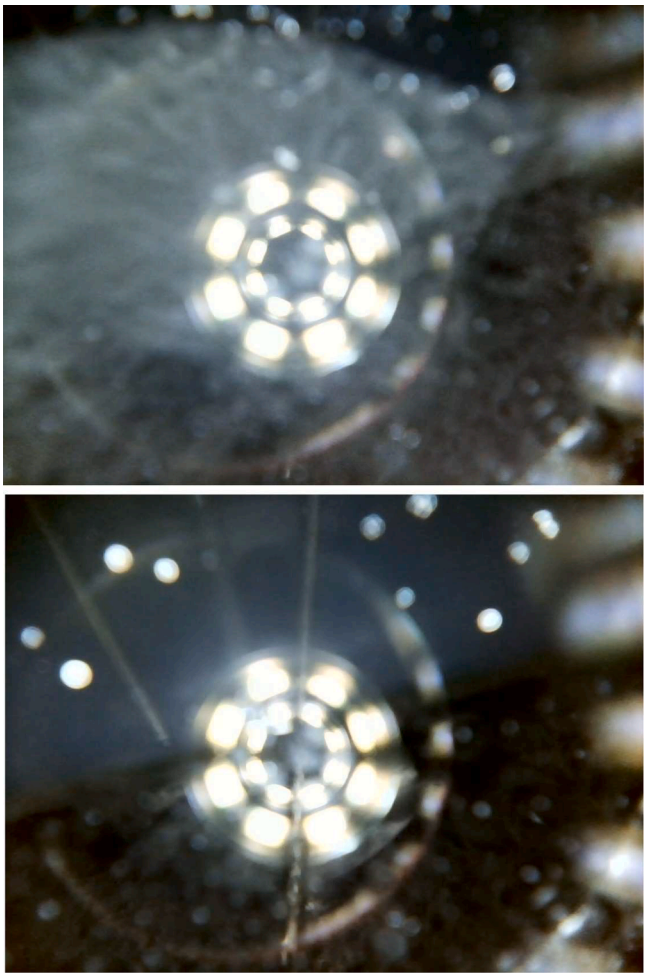

Fig. 3. Insight view of the VLE cell. 800 RPM (vortex – upper image) vs. 400 RPM (smooth – lower image).

Sampling

When the VLE is established, the stirrer is stopped, and a sample can be taken. Before the final sample is sent for analysis, the sample cylinder and the line to the GC is flushed and evacuated three times with gas from the cell. For each flushing, the stirrer is kept running and the equilibrium is reestablished by the operation of the bellows inside the cell. The sample is first transferred to a sample cylinder to protect the GC against high pressure. This procedure is automated and controlled by the software. The pressure inside the sample cylinder is measured by a pressure sensor. The sample cylinder is filled with gas to the pressure of 2 bar. The sample is also transferred to sample cylinder at 2 bar. When the GC is ready (column temperature reaches 100 °C), the sample is sent to the GC for analysis. During the analysis, the sampling cylinder and tubing from the VLE cell to the GC are evacuated, as a preparation for the next sample. The bellows are moved to a low volume position and CO_2 is injected into the cell to a pressure slightly below the measurement pressure. The procedure is repeated for at least 7 samples. For the analysis, the minimum and maximum values of each measurement are then excluded. Extended graphical interpretation can be seen in Fig. 4.

Uncertainty analysis

The uncertainty analysis was performed for the pressure, temperature and concentration measurements. Density measurements were not performed, as the apparatus was not designed for those measurements. Also, at some point, there was a limitation in the gravimetrical separation in some regions of the CO_2-water mixture due to similar density.

Pressure

The uncertainty analysis is based on the terms and definition of JCGM 100 (2008) and former studies in our laboratory reported by Westman et al. (2016). The resulting uncertainty in pressure is constant for the different pressure transducers in use, since the dominating error is given as a function of the full scale. The impact on the concentration is calculated from an estimate of the derivative in the measurement point.

Temperature

The temperature sensor T-05 is a standard platinum resistance thermometer (SPRT), calibrated from reference temperatures given by the International Temperature Scale of 1990 (ITS-90). The method used is equivalent to the method used by Westman et al. (2016) with an extension to the calibration at higher reference temperatures for Indium and Tin. The temperature sensor T-04 is a PT-100 and it is calibrated against the same reference temperatures. For the two dependent temperature measurements the uncertainty in the measured temperature is:

$$u(T_{Stat}) = \left| u(T_{04}) \frac{\partial T}{\partial T_{04}} \right| + \left| u(T_{05}) \frac{\partial T}{\partial T_{05}} \right| = \left| \frac{u(T_{04})}{2} + \frac{u(T_{05})}{2} \right|$$

In addition, minor temperature fluctuations in the cell can be observed due to stirring and sampling. The measured fluctuations are less than 15mK. This variation occurs inside the steel wall, while the processes causing the fluctuations occur in the fluid mixture. There is a temperature increase due to the stirring, and a temperature drop due to the sampling from the cell. Heat transfer calculations indicate that the temperature change in the cell is twice as large as the observed temperature change in the cell wall. The uncertainty in the temperature measurement is therefore corrected to include this factor as follows:

$$u(T(t)) = \sqrt{\sum_{i=1}^{n} \frac{(\overline{T} - T_i)^2}{n-1}}$$

To account for this, an additional term described by the standard deviation of the observed temperatures is added to the uncertainty in the

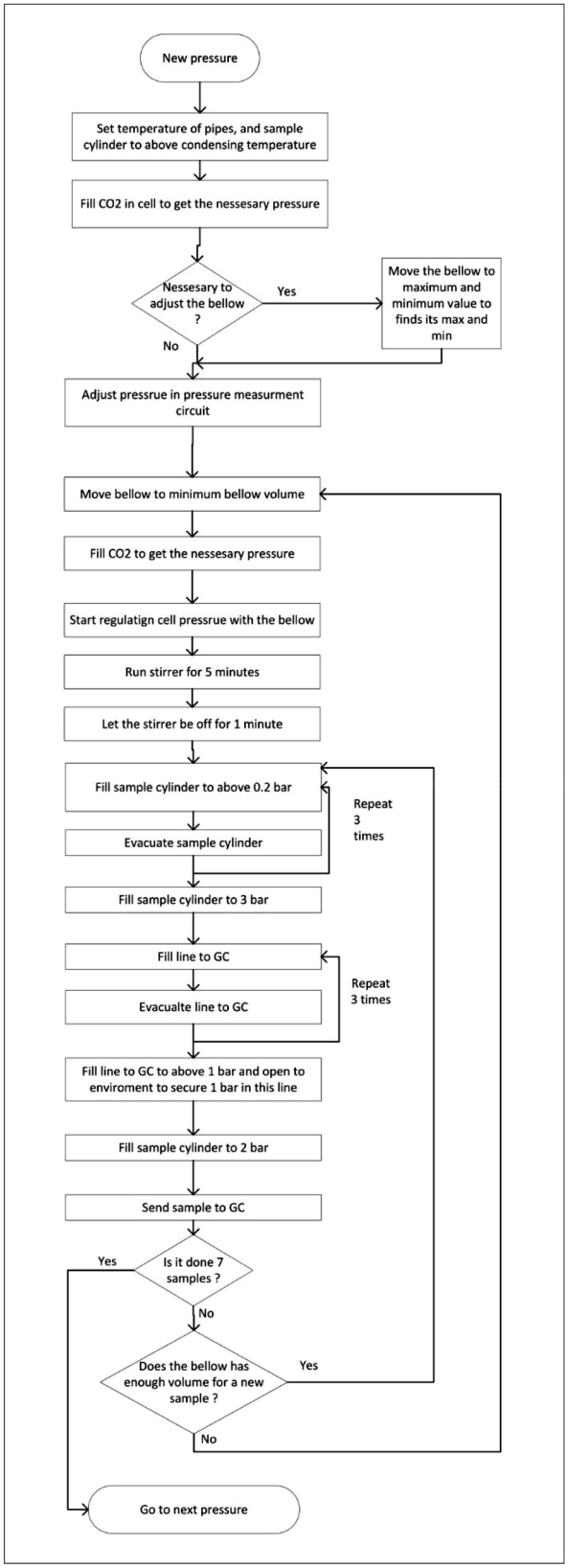

Fig. 4. Block diagram of sampling.

measurement system:

$$u(T) = \sqrt{u(T_{Stat})^2 + u(T(t))^2}$$

It is dominated by the temperature instability and set as the maximum fluctuation for all the measurements.

Concentration measurement

The uncertainty in the composition measurement is dominated by the production of the calibration gas used to determine the relative response factor for the GC. The uncertainty for the concentration measurement is estimated to be equal to the uncertainty in the gravimetrical preparation of the calibration gas at 0.5 % (mol) H_2O in CO_2 for all the measurements where the concentration is below 0.65 %, and equal to the uncertainty for the gravimetrical preparation of the calibration gas at 2 % (mol) H_2O in CO_2 for the measurements above 1 %.

Results and discussion

The experiment was performed at the isotherm of 50 °C and pressures between 1 and 17.5 MPa, the results are presented in Table 2. X_{H2O} is an average value for the vapour samples in 5 measurements at 7 measurement points – with minimum and maximum values excluded. The isotherm of 50 °C was selected to validate the setup. The authors are aware that higher temperatures were reached in the EGS reservoir, however, the more sensitive region in terms of the change of the shape of the dew line was found for lower temperatures. The reason is the focus on injection purposes rather than reservoir conditions. During production, temperature and pressure drops can occur, following the change of the dew curve, which is more important for the top part of the system compared to actual reservoir conditions. A greater percentage error in the region of sCO_2 pressures shows the difficulty of the measurements. The next desired pressure point was set to 50 MPa, however, such pressure values were not achieved in practice, even if the pump is designed to work up to 100 MPa. The possible reason was insufficient pressure in the gas cylinder (the source of CO_2) and the low volume of the syringe pump that could not increase the pressure to the expected value. The authors wished to provide more data, however, the results gained in this paper are the first collected for this apparatus and much time was spent upgrading the setup in a proper way. Also, the lack of more data is affected by the limited time for study. However, based on the very high precision at higher pressures, authors believe that further research will bring very accurate data for CO_2–H_2O and other mixtures.

Points are presented in Fig. 5 with a comparison to literature data gained by Spycher et al. (2003), Coan and King (1970), Hou et al. (2013) and the TREND (GERG-2008/EOS-CG) equation of state by Span et al. (2020).

As mentioned earlier, the data collected by HPC-PE are the first results of this facility. The results obtained during the experiment and their fit to established literature confirm the appropriate design of the apparatus and sufficiently skilful operation, however, the VLE at higher temperatures and pressures is expected to be checked and validated. Pressure points were chosen in a way to not repeat the same pressure points collected by other researchers, but also to collect new ones and assemble them together to increase the accuracy of the equation of state. The increment was not regular, and more measurements were conducted close to the critical pressure of CO_2, where a “bend” in the meander is observed. The mole fraction of water rapidly decreases as the pressure increases and stabilises around 7.5 MPa. Above that pressure, the mole fraction increases, however, the change is not so rapid, and its rate decelerates between 10 and 12.5 MPa. VLE behaviours at the pressures between 6 and 8.4 MPa are very similar and correlate with data collected by Spycher et al. (2003) and Hou et al. (2013). The shift of the point collected at 7.8 MPa is interesting in terms of the change of CO_2 state from gaseous to supercritical, where the mole fraction of water

Table 2
VLE results of CO_2—H_2O system at isotherm of 50 °C.

	Data			Analysis statistics		Accuracy against GERG-2008		Uncertainty			Total uncertainty	
	T	P	X_{H2O}	SD	CV	Absolute error	Percentage error	u(T)	u(P)	u(X_n)	u (X_n)	u_r (X_n)
Unit	K	MPa	%	%	%	%	%	mK	kPa	ppm	ppm	%
G1	323.495	1.001	1.3075	–	–			31	0.4	12	24	0.19
G2	323.343	3.501	0.4833	0.004	1.015	0.021	4.145	31	1.3	42	42	0.87
G3	323.353	6.001	0.3585	0.004	1.212	0.031	7.855	31	1.3	26	26	0.74
G4	323.349	7.301	0.3541	0.007	2.215	0.033	8.505	31	1.3	45	45	1.28
G5	323.348	7.801	0.3481	0.003	0.876	0.042	10.683	31	1.3	19	19	0.55
G6	323.351	8.401	0.3577	0.004	1.348	0.,041	10.336	31	1.3	23	23	0.65
G7	323.347	12.000	0.5404	0.005	1.012	0.027	4.771	31	2.5	38	38	0.71
G8	323.347	17.499	0.6491	0.017	2.894	0.007	1.044	31	2.5	137	137	2.12

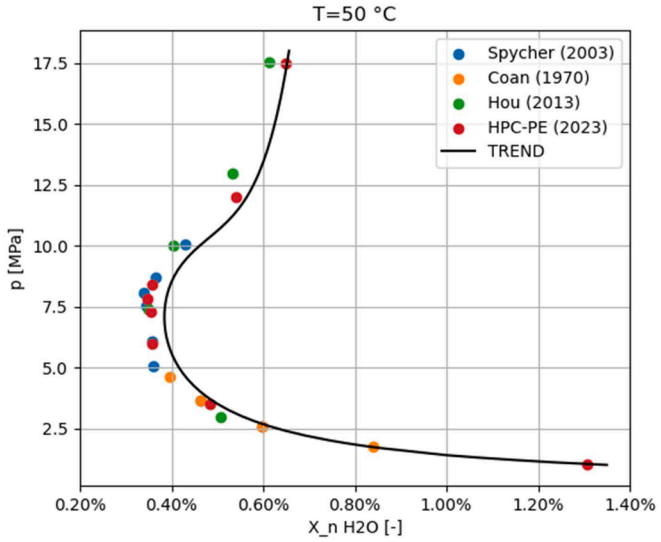

Fig. 5. Experimental data compared with literature data and TREND.

is the lowest among all the results. It is also interesting that the TREND equation does not provide a similar shift and leans into the other side, with an increased mole fraction of water. The lowest and highest points of this study overlap with the TREND equation. The precision of the measurements in comparison to the GERG-2008/EOS-CG is low in a close region of the critical pressure of sCO_2. Values around 10 % of percentage error are high, but absolute error is not so. What is more, none of the cited research teams get nearer with their results in critical region and above it. Also, a low total uncertainty confirms the well performed operation of the testing setup and the stability of the results. A good fit to the literature (Hou et al., 2013; Spycher et al., 2003; Coan and King, 1970) and TREND (Span et al., 2020) at 50 °C is promising for filling current knowledge gaps and data points at higher pressures and isotherms, for instance in a temperature range from 150 to 200 °C and up to 1000 bar in pressure, the maximum working conditions of HPC-PE and typical EGS conditions.

Existing studies confirm the extreme difficulty of achieving reliable results at high pressures and temperatures. Also, in this case, the implementation of the experimental campaign proved to be a very challenging task. The data obtained by the HPC-PE are the first very promising results from this instrument. The HPC-PE is ideal for this type of measurements, nevertheless, some difficulties were encountered in preparing for testing and then obtaining results for the 150 °C isotherm, which would be of great interest for a CO_2- Enhanced Geothermal System.

The new data obtained in this study may influence the change for further updates in the equations of state for CO_2 and water mixtures. Further development of CO_2-Enhanced Geothermal System is also expected as a result of this study. The benefits of this study for EGS technology include the materials and parts selections for topside systems. A future designer should pay attention to the fluid appliaction in direct and indirect injection to the turbine. Also, a dryer or separator can be installed in the cycle, however, this would result in a pressure drop. More information about the design, fluid parameters and integration is still required.

Conclusion

A new measurement apparatus for accurate measurement of high-pressure and high-temperature phase equilibrium is described. The vapour concentration for the CO_2—H_2O system is reported for an isotherm at 323 K and pressures from 1 to 17.5 MPa.

The data points reported in this study are consistent with literature data as presented in Table 2 and Fig. 5. Compared with the GERG-2008/EOS-CG, the measured H_2O concentration is lower than the concentration predicted from TREND.

Overall, the apparatus produces satisfactory measurements, there are possible improvements in the stirring and sampling procedure to achieve better temperature stability in the measurement volume. Improvements in increasing the temperature and pressure are also expected.

CRediT authorship contribution statement

Jacob Stang: Writing – review & editing, Writing – original draft, Supervision, Resources, Methodology, Data curation, Conceptualization. **Anders Austegard:** Writing – original draft, Visualization, Validation, Supervision, Software, Resources, Methodology, Investigation, Formal analysis, Data curation, Conceptualization. **Yannick Jooss:** Writing – original draft, Visualization, Investigation, Formal analysis. **Maciej Szymanek:** Writing – review & editing, Writing – original draft, Visualization, Validation, Investigation, Formal analysis, Data curation. **Anna Sowiżdżał:** Writing – review & editing, Writing – original draft, Project administration, Funding acquisition.

Declaration of competing interest

The authors declare that they have no known competing financial interests or personal relationships that could have appeared to influence the work reported in this paper.

Data availability

Repository data.

Acknowledgment

The research leading to these results has received funding from the Norway Grants 2014–2021 via the National Centre for Research and Development. The results are part of the Polish-Norwegian project: CO_2-

Enhanced Geothermal Systems for Climate Neutral Energy Supply, acronym EnerGizerS, registration number NOR/POLNOR/EnerGizerS/0036/2019.

Research project partly supported by program "Excellence initiative – research university" for the AGH University of Krakow.

Appendix

Calibration

Temperature calibration

Temperature measurements are performed using a glass capsule 25 Ω Standard Platinum Resistance Thermometer (model 5686-B, HS333, supplied by Fluke Calibration) mounted in the hole on the top/bottom and 100 Ω Platinum Resistance Thermometer (model 5615–9-B) s/n 1,032,663, supplied by Fluke Calibration) mounted on the top/bottom of the cell. The SPRT covers temperature from -260 °C to 232 °C and its accuracy and reproducibility is ± 1 mK. The PT-100 covers temperatures from -196 °C to 420 °C and its accuracy is 12 mK at 0 °C. Two temperature sensors allow to control both the vapour and the liquid phases independently. Current signals from SPRT and PT-100 are measured and the ratio between its resistance and reference resistor are converted to temperature readings.

Both SPRT and PT-100 were calibrated by the supplier, but in order to reduce the uncertainty, a second calibration was performed in SINTEF. For this purpose, three fixed point cells according to the international temperature scale of 1990 (Preston-Thomas, 1990) were used:

- Freezing point of tin (231.928 °C)
- Freezing point of indium (156.5985 °C)
- Tripple point of water (0.01 °C)

Temperature calibrations were performed according to NIST recommendations described by Strouse (2007) and supplier of SPRT – Fluke Calibration recommendations, described by Li et al. (2005) using three fixed point cells: freezing point of tin, freezing point of indium and triple point of water. The differences are the use of oil bath instead of a furnace and stainless-steel rods instead of fused-silica rods. Both SPRT and PT-100 were calibrated on the same freezing/triple plateau. Data analysis followed (BIPM, 2018a; BIPM, 2018b) and is presented in Tables 3 and 4.

Table 3
The defining fixed points of the ITS-90 and results of the calibration of SPRT.

Fixed point	State	ITS 90 temperature [°C]	ITS 90 temperature [K]	$Wr(T_{90})$	u (T_{90}) [mK]	$W(T_{90})$ $I = 0$mA	$\Delta W(T_{90})$	T[°C]	Polynominal fit [mK]
Tin	FP	231.928	505.078	1.8928	0.6 (0.2)	1.89266	-0.00013	231.892	37.8876
Indium	FP	156.5985	429.749	1.6098	0.8 (0.2)	1.60974	-6.2E-05	156.582	17.3585
Water	TP	0.01	273.16	1	0.05 (0.03)	1.00007	7.2E-05	0.02806	-18.0575

Table 4
The defining fixed points of the ITS-90 and results of the calibration of PT-100.

Fixed point	State	ITS 90 temperature [°C]	ITS 90 temperature [K]	$Wr(T_{90})$	u (T_{90}) [mK]	$W(T_{90})$ $I = 0$mA	$\Delta W(T_{90})$	T[°C]	Polynominal fit [mK]
Tin	FP	231.928	505.078	1.8928	0.6 (0.2)	1.89245	-0.00035	231.834	92.9795
Indium	FP	156.5985	429.749	1.6098	0.8 (0.2)	1.60955	-0.00025	156.532	66.0358
Water	TP	0.01	273.16	1	0.05 (0.03)	0.99992	-8.3E-05	-0.01091	20.9114

Where:
FP – freezing point
TP – triple point
$Wr(T_{90})$ – reference function value at temperature T
$U(T_{90})$ – the smallest uncertainty estimates claimed by metrological institutes
$W(T_{90})$ – resistance ratio at temperature T
$\Delta W(T_{90})$ – deviation of W from reference function at temperature T
T – temperature of freezing/triple point from calibration
Polynominal fit – deviation value at temperature T
Based on the results presented above, calibration deviation function for SPRT and PT-100 are described by the formulas:

$$SPRT\ (\Delta T) = 1.5861\ x^2 + 19.492\ x - 18.063$$

$$PT100\ (\Delta\ T) = 3.2639\ x^2 + 24.131\ x + 20.194$$

Where x is T[°C]/100.

Pressure calibration

Pressure sensors were calibrated by the supplier, however, a second calibration was performed in the SINTEF lab using a dead-weight tester (Desgranges et Huot, model 26000 M) and accurate weights with a well-known wetted area (Løvseth, 2022), to correct the drift and increase the

precision of measurements.

Pressure sensors were calibrated according to the manual of the deadweight tester (Desgranges et Huot, model 26,000 M). In the beginning, 5 metal plates with certified weight were put on the deadweight tester and checked. Then, special piston cells (supplied by IKM Laboratorium AS – Tananger) with maximum working pressure of 10, 50 and 200 bar, respectively, were used. Lab conditions such as room temperature, atmospheric pressure, humidity, and temperature of the piston cell were taken into account during calibration. Atmospheric pressure was measured by a Paroscientific INC Digiquartz barometer, model 710, while room temperature and humidity were measured by the THB P thermohygrobarometer from the RADWAG WAY 1.4Y.KO system. The temperature of the piston cell was measured using the Agilent Technologies Data Acquisition/Switch Unit, 20 Channel Multiplexer, model 34970A. All pressure transmitters were calibrated against several fixed pressures, depending on the piston cell. For the 10 bar cell, 3 fixed pressures were measured: 1, 3 and 9 bar, respectively. For the 50 bar cell, 4 fixed pressures were measured: 9.5, 20, 29.5 and 50 bar, respectively. Finally, for the 200 bar cell, 6 fixed pressures were measured: 50, 70, 90, 120, 150, 175 bar, respectively. Based on the results, the difference between absolute and manometric pressure was calculated. The difference against absolute pressure for each transmitter at fixed pressures was mapped and curve fitting was performed. Because of the limited range of piston cells, curve fitting enabled the extrapolation and evaluation of the limit pressure. Most of the fitting curves were quadratic and were chosen due to their coefficient of determination.

In Table 5, pressure functions and coefficient of determination R^2 are presented:

Table 5
Details of pressure calibration functions.

Pressure transmitter (max range)	PT-01 (10 bar)	PT-02 (30 bar)	PT-03 (100 bar)	PT-04 (200 bar)	PT-05 (500 bar)	PT-06 (1000 bar)
R^2	0.787	0.901	0.816	0.753	0.966	0.764
F	Y = 1.5282E-04x+1.8515E-03	Y=-3.2351E-06x^2+8.6713E-06x+2.3809E-03	Y=-19883E-06x^2+1.766E-04+5.5335E-03	Y=-1.5793E-06x^2+2.2899E-04x+1.9052E-02	Y=-1.9824E-04x+1.6113E-01	Y=-8.008E-05x+1.6315E-01

Mixture preparation and GC calibration

The GC was calibrated against 3 gas mixtures prepared gravimetrically in the SINTEF laboratories. The TREND equation of state tool was used to select the composition of mixtures (0.995, 0.98, 0.9 and 0.7 mole fraction of CO_2) and to calculate the masses of components to protect the special cylinders against high pressure (Swagelok Sample cylinder- 304lSS with a volume of 3.785 l – with sulfinated surface treatment). A specifically designed set-up for gravimetrically preparing the calibration gases was used. The setup and the general procedure were described in more details by Westman et al. (2014). This procedure was slightly adapted for the use of H_2O as one of the components and different gas cylinders were used. H_2O was purified by a Merck Milipore Direct-Q® 3 Water Purification System and then filled into the previously gas cylinder at a state of vacuum. To avoid any contamination by air leakage into the gas cylinder during the H_2O filling procedure, the gas cylinder was always purposely filled above the desired H_2O mass during the first step. Then, in a second step, the gas cylinder was connected to a vacuum pump to evacuate all possible contaminants until the target H_2O mass was reached by evaporation and evacuation of the H_2O. In addition to avoiding undesired contaminants, this method also enabled a very precise filling of the desired H_2O mass. The target mass of CO_2 was then recalculated and injected. After H_2O and CO_2 filling, some waiting time was included to assure thermodynamic equilibrium was reached before weighing the cylinder.

Finally, the calibration cylinders were heated to reach uniform gas phase. For that purpose, each cylinder was put on a roller machine and heated to 200 °C for more than 24 h. Then, hot gas phase was transferred to the GC, where water and CO_2 were separated, and the composition was checked. At least 7 samples from every mixture were sent, checked and standardised. Based on the mole fraction and area fraction, a response factor was calculated to provide for a proper transition between area fraction and mole fraction. In actual measurements of the VLE, area fraction could be obtained by conversion and the mole fraction would be known.

References

Aasen, A., Hammer, M., Skaugen, G., Jakobsen, J., Wilhelmsen, Ø., 2017. Thermodynamic models to accurately describe the PVTxy-behavior of water/carbon dioxide mixtures. Fluid Phase Equilib. 442, 125–139. https://doi.org/10.1016/j.fluid.2017.02.006 ss.

Aminu, M.D., Nabavi, S.A., Rochelle, C.A., Manovic, V., 2017. A review of developments in carbon dioxide storage. Appl. Energy 208, 1389–1419. https://doi.org/10.1016/j.apenergy.2017.09.015.

Bureau International des Poids et Mesures. 2018a. Guide to the Realization of the ITS-90. Introduction.

Bureau International des Poids et Mesures. 2018b. Guide to the Realization of the ITS-90. Platinum Resistance Thermometry.

Caumon, M.C., Sterpenich, J., Randi, A., Pironon, J., 2016. Measuring mutual solubility in the H2O–CO2 system up to 200bar and 100°C by *in situ* Raman spectroscopy. Int. J. Greenh. Gas Control 47, 63–70. https://doi.org/10.1016/j.ijggc.2016.01.034 ss.

Coan, C.R., King Jr, A.D., 1970. Solubility of water in compressed carbon dioxide, nitrous oxide, and ethane. Evidence for hydration of carbon dioxide and nitrous oxide in the gas phase. J. Am. Chem. Soc. 93 (8), 1857–1862. https://doi.org/10.1021/ja00737a004, 1971.

Cui, G., Ren, S., Rui, Z., Ezekiel, J., Zhang, L., Wang, H., 2018. The influence of complicated fluid-rock interactions on the geothermal exploitation in the CO2 plume geothermal system. Appl. Energy 227, 49–63. https://doi.org/10.1016/j.apenergy.2017.10.114.

Dohrn, R., Peper, S., Fonseca, J., 2010. High-pressure fluid-phase equilibria: experimental methods and systems investigated (2000-2004). Fluid Phase Equilib. 588, 1–54. https://doi.org/10.1016/j.fluid.2009.08.008 ss.

ECCSEL ERIC. (2023, April). HPC-PE (NO2.7) Facility for high pressure or complex phase equilibrium measurements. https://www.eccsel.org/catalogue/169.

Gładysz, P., Sowiżdżał, A., Miecznik, M., Pająk, L., 2020. Carbon dioxide-enhanced geothermal systems for heat and electricity production: energy and economic analyses for central Poland. Energy Convers. Manag. 220, 113142 https://doi.org/10.1016/j.enconman.2020.113142.

Honarvar, B.B., Sajadian, S.A., Sepúlveda, A.R., Galotto, M.J., Jouyban, A., 2023. Solubility and thermodynamic modeling of sildenafil citrate in supercritical carbon dioxide. Fluid Phase Equilibria 566, 113677. https://doi.org/10.1016/j.fluid.2022.113677. Volume.

Hou, L., Yu, Z., Luo, X., Wu, S., 2022. Self-sealing of caprocks during CO2 geological sequestration. Energy 252, 124064. https://doi.org/10.1016/j.energy.2022.124064. Volume.

Hou, S.X., Maitland, G.C., Trusler, J., 2013. Measurement and modeling of the phase behavior of the (carbon dioxide+water) mixture at temperatures from 298.15K to 448.15K. J. Supercrit. Fluids 73, 87–96. https://doi.org/10.1016/j.supflu.2012.11.011 ss.

JCGM 100:2008. GUM 1995 with minor corrections. Evaluation of measurement data – Guide to the expression of uncertainty in measurement.

Kim, C., Chun-Jae, Y., Hyung-Suk, O., Byoung, K.M., Ung, L., 2022. Review of carbon dioxide utilization technologies and their potential for industrial application. J. CO2 Util. 65, 102239 https://doi.org/10.1016/j.jcou.2022.102239.

Løvseth, S.W. (2021). D. 3.1. Deliverable report. Prioritized measurement Plan. Trondheim. [unpublished].

Løvseth, S.W., 2022. M3.2 Milestone report. Calibration of Equipment Complete. Trondheim. [unpublished].

Leventaki, E., Baena-Moreno, F.M., Wojtasz-Mucha, J., Sjostedt, N., Tajik, A.R., Sardina, G., Strom, H, Bernin, D., 2023. Experimental evaluation of black liquor

carbonation for carbon dioxide capture. J. CO2 Util. 72, 102516 https://doi.org/10.1016/j.jcou.2023.102516.

Li, X., Zhao, M., Chen, D., 2005. Realization of the freezing points of indium, tin and zinc using stainless steel-cased cells. Hart Sci. Hentet March 2022 https://eu.flukecal.com/literature/articles-and-education/temperature-calibration/papers-articles/realization-freezing-point.

Noorani, N., Mehrdad, A., Ahadzadeh, I., 2021. CO2 absorption in amino acid-based ionic liquids: experimental and theoretical studies. Fluid Phase Equilib. 547, 113185 https://doi.org/10.1016/j.fluid.2021.113185.

Olasolo, P., Juárez, M.C., Morales, M.P., Olasolo, A., Agius, M.R., 2018. Analysis of working fluids applicable in Enhanced Geothermal Systems: nitrous oxide as an alternative working fluid. Energy 157, 150–161. https://doi.org/10.1016/j.energy.2018.04.006.

Pająk, L., Sowiżdżał, A., Gładysz, P., Tomaszewska, B., Miecznik, M., Andresen, T., Frengstad, B.S., Chmielowska, A., 2021. Multi-criteria studies and assessment supporting the selection of locations and technologies used in CO2–EGS systems. Energies 14, 7683. https://doi.org/10.3390/en14227683 (Basel).

Preston-Thomas, H., 1990. The international temperature scale of 1990 (ITS-90). Metrologia (27), 3–10. https://doi.org/10.1088/0026-1394/27/1/002 ss.

Pruess, K., 2008. On production behavior of enhanced geothermal systems with CO2 as working fluid. Energy Convers. Manag. 49, 1446–1454.

Sowiżdżał, A., Gładysz, P., Andresen, T., Miecznik, M., Frengstad, B.S., Liszka, M., Chmielowska, A., Gawron, M., Løvseth, S.W., Pająk, L., et al., 2021. CO2-enhanced geothermal systems for climate neutral energy supply. In: Proceedings of the TCCS-11-Trondheim Conference on CO2 Capture, Transport and Storage. Trondheim, Norway. https://hdl.handle.net/11250/2786085.

Span, R., Beckmüller, R., Hielscher, S., Jäger, A., Mickoleit, E., Neumann, T., Pohl, S.M., Semrau, B., Thol, M., 2020. TREND. Thermodynamic Reference and Engineering Data 5.0. Lehrstuhl für Thermodynamik, Ruhr-Universität Bochum.

Spycher, N., Pruess, K., Ennis-King, J., 2003. CO_2-H_2O mixtures in the geological sequestration of CO2. I. Assessment and calculation of mutual solubilities from 12 to 100°C and up to 600 bar. Geochim. Cosmochim. Acta 67 (16), 3015–3031. https://doi.org/10.1016/S0016-7037(03)00273-4.

Stang, J., Løvseth, S.W., Størset, S.Ø., Malvik, B., Håvard, R., 2013. Accurate measurements of CO2 rich mixture phase equilibria relevant for CCS transport and conditioning. Energy Procedia 37, 2897–2903. https://doi.org/10.1016/j.egypro.2013.06.175 ss.

Strouse, G.F., 2007. Standard Platinum Resistance Thermometer Calibrations from the Ar TP to the Ag FP. National Institute of Standards and Technology, Gaithersburg, MD, pp. 250–281. https://doi.org/10.6028/NIST.SP.250-81. Vol. NIST Special Publication.

Tabasinejad, F., Moore, R.G., Mehta, S.A., Van Fraassen, K.C., Barzin, Y., Rushing, J.A., Newsham, K.E., 2011. Water solubility in supercritical methane, nitrogen, and carbon dioxide: measurement and modeling from 422 to 483 K and pressures from 3.6 to 134 MPa. Ind. Eng. Chem. Res. (50), 4029–4041. https://doi.org/10.1021/ie101218k ss.

Tagliaferri, M., Gładysz, P., Ungar, P., Strojny, M., Talluri, L., Fiaschi, D., Manfrida, G., Andresen, T., Sowiżdżał, A., 2022. Techno-economic assessment of the supercritical carbon dioxide enhanced geothermal systems. Sustainability 14, 16580. https://doi.org/10.3390/su142416580.

Tester, J.W., Anderson, B.J., Batchelor, A.S., Blackwell, D.D., Dipippo, R., Drake, E.M., Garnish, J., Livesay, B., Moore, M.C., Nichols, K., Petty, S., Toksoz, M.N. & Veatch, R.W., 2006. The future of geothermal energy. Impact of enhanced geothermal systems (EGS) on the United States in the 21st Century. Massachusetts Institute of Technology ISBN: 0-615-13438-6.

Wang, Z., Zhou, G., Guo, H., Yang, P., Lu, W., 2018. Determination of water solubility in supercritical CO2 from 313.15 to 473.15 K and from 10 to 50 MPa by *in-situ* quantitative Raman spectroscopy. Fluid Phase Equilib. 476, 170–178. https://doi.org/10.1016/j.fluid.2018.08.006 ss.

Westman, S.F., Stang, J., Størset, S.Ø., Rekstad, H., Austegard, A., Løvseth, S.W, 2014. Accurate phase equilibrium measurements of CO2 mixtures. Energy Procedia 51, 392–401. https://doi.org/10.1016/j.egypro.2014.07.046 ss.

Westman, S.F., Stang, H.G.J., Løvseth, S.W., Austegard, A., Snustad, I., Ertesvåg, I.S., 2016. Vapor-liquid equilibrium data for the carbon dioxide and oxygen (CO_2+O_2) system at the temperatures 218, 233, 253, 273, 288 and 298 K and pressures up to 14 MPa. Fluid Phase Equilib. 421, 67–87. https://doi.org/10.1016/j.fluid.2016.04.002.

Zhang, F.Z., Xu, R.N., Jiang, P.X., 2016. Thermodynamic analysis of enhanced geothermal systems using impure CO_2 as the geofluid. Appl. Therm. Eng. 99, 1277–1285. https://doi.org/10.1016/j.applthermaleng.2016.01.126 volpages.